Lithos 320–321 (2018) 62–74

Contents lists available at ScienceDirect

Lithos

journal homepage: www.elsevier.com/locate/lithos

Petrogenesis of Triassic granite from the Jintan pluton in Central Jiangxi Province, South China: implication for uranium enrichment

Jihua Tao [a,b,c,*], Wuxian Li [b], Derek A. Wyman [c], Andong Wang [a], Zhitian Xu [d]

[a] Fundamental Science on Radioactive Geology and Exploration Technology Laboratory, East China University of Technology, Nanchang 330013, China
[b] State Key Laboratory of Isotope Geochemistry, Guangzhou Institute of Geochemistry, Chinese Academy of Sciences, Guangzhou 510640, China
[c] School of Geosciences, The University of Sydney, Sydney 2006, Australia
[d] Geologic Party No.293, Guangdong, Nuclear Industry Buerau, Guangzhou 510800, China

ARTICLE INFO

Article history:
Received 27 March 2018
Accepted 4 September 2018
Available online 7 September 2018

Keywords:
Triassic granite
Jintan pluton
S-type granite
U-rich granite
South China

ABSTRACT

Numerous Triassic biotite granites and two-mica granites crop out in the interior of South China, and some of them possess high U contents, which have been regarded as the sources for later hydrothermal mineralization. Their petrogenesis is therefore crucial for constraining the possible origins of the U enrichment. Here we report new LA-ICPMS zircon U—Pb ages, mineral geochemistry of biotite and muscovite, whole rock geochemical results and Sr—Nd and zircon Hf isotope data from the Jintan pluton in Central Jiangxi Province, South China. LA-ICPMS zircon U—Pb dating indicates that both biotite granite (BG) and two-mica granite (TMG) in the Jintan pluton crystallized at ~220 Ma. The TMG have higher U contents (7.85 to 48.90 ppm, average18.44 ppm) than theBG (4.99 to 17.72 ppm, average 8.64 ppm). Both BG and TMG show negative whole-rock $\varepsilon_{Nd}(t)$and zircon $\varepsilon_{Hf}(t)$values and contain some inherited zircons. The TMG are strongly peraluminous (A/CNK = 1.13–1.33), contain abundant primary muscovite, and display S-type affinity on plots of Y*vs* Rb and Th *vs* Rb, suggesting that they are S-type granites. The BG also display S-type granite affinities on plots of Y*vs* Rb and Th *vs* Rb. The suites display similar Sr—Nd isotope compositions (BG initial $^{87}Sr/^{86}Sr$ values = 0.711389 to 0.714225 and $\varepsilon_{Nd}(t) = -9.91$ to −9.16, TMG initial $^{87}Sr/^{86}Sr$ values = 0.711832 and $\varepsilon_{Nd}(t) = -10.02$) and are spatially associated, suggesting that the BG should also be classified as S-type granites. The TMG have higher zircon εHf(t)values (−6.4 to −1.1) than the BG (−8.7 to −3.7), indicating the TMG and BG might be derived from similar sediments but possibly with some distinct characteristics in their sources. The BG exhibit linear covariations in chemical compositions with relatively high total REE and light REE contents and MgO contents, while the TMG displays broader compositional variations but with relatively low total REE, light REE and MgO contents. Biotite geochemistry indicates the TMG formed in a more reduced magmatic system than the BG. The temperatures estimated by zircon saturation thermometry indicate the BG had distinctly higher magmatic temperatures than the TMG. The TMG display relatively high Al_2O_3/TiO_2 ratios and low CaO/Na_2O ratios than the BG but have higher Sr/Y and La/Yb ratios. The geochemical and petrological data suggest the BG were derived from clay-poor psammite sources at deeper levels with higher temperatures and higher oxygen fugacity, and underwent an extensive fractional crystallization, while the TMG was derived from clay-rich pelitic sources at higher levels and lower temperatures and oxygen fugacity with only limited fractional crystallization. We conclude that the combination of U-rich sources, physical-chemical conditions such as low partial melting temperature or low degrees of partial melting, a reduced environment and low REE and LREE contents of magmas controlled the U enrichment in TMG.

1. Introduction

Granite is the most important constituent of upper continental crust and can form in various tectonic settings (Brown, 2013; Jiang and Zhu, 2017). Deciphering the origin of granites has great bearing on our understanding of continental differentiation and their genetic links to mineralization (Gao et al., 2018 and references therein). The Triassic granites in the interior of South China have been regarded as the product of intracontinental orogeny (Gao et al., 2017; Li and Li, 2007; Wang et al., 2013; Zhao et al., 2016; Zhou et al., 2006) and some of the intrusions are closely related to polymet allic mineralization in the region (Hu et al., 2017). Previous studies have shown that these granites are dominantly S-type with only minor I-type and A-type granites being present (Chen et al., 2007; Wang et al., 2013; Zhao et al., 2013a; Zhao et al., 2017; Zhou et al., 2006). Gao et al. (2017) have recently proposed that the granites can be categorized into five groups: cordierite-bearing granites, amphibole-bearing granites, biotite granites,

* Corresponding author.
E-mail address: taojihua123@163.com (J. Tao).

https://doi.org/10.1016/j.lithos.2018.09.003
0024-4937/

muscovite-bearing granites, and A-type granites. The cordierite-bearing granites and muscovite-bearing granites have already been recognized as S-type granite (Qi et al., 2007) while the amphibole-bearing granites are I-types(Chen et al., 2007; Zhao et al., 2017). The biotite granites have been characterized as either I-type granite or S-type granite (Zhou et al., 2006). Overall, S-type granites are the volumetrically dominant type of granite in South China. Biotite and muscovite-bearing granites usually coexist with each other in a single pluton, which raises the question of the genetic relationship between the two granite types.

Moreover, previous studies demonstrated that some of the Triassic granites have high U contents and play an important role in the formation of hydrothermal uranium deposits (Chen, 2004; Chen et al., 2012; Dong et al., 2010; Zhao et al., 2016). Although the deposits may be hosted in either granites or volcanic rocks, most of the basement or wall rocks in the vicinity of the deposits are U-rich Triassic granites (Chen, 2004; Chen et al., 2012; Dong et al., 2010; Zhao et al., 2016). Nevertheless, the primary U enrichment mechanism in Triassic granites is still a matter of debate. For instance, Dong et al. (2010) concluded that multi-stage metamorphism and re-melting resulted in uranium enrichment in some granites. Zhao et al. (2011) and Zhao et al. (2016) suggested that a distinct U-rich source may be the key factor in the generation of peraluminous U-bearing granites in South China. Alternatively, Chen et al. (2012) and Zhang et al. (2017) proposed that magma differentiation, plus specific physical-chemical conditions (such as temperature, volatile components and oxidation state) resulted in higher U content. Interestingly, many of the U-rich Triassic granites are S-types derived from sedimentary sources (Chen et al., 2012; Dong et al., 2010; Zhao et al., 2013b, 2016) and it is therefore important to study these rocks to better define uranium exploration criteria in South China and worldwide.

The Jintan pluton is a Triassic S-type granite intrusion in the Central Jiangxi Province, South China that contains both biotite and two-mica granite (JGS, 1984; Zhao et al., 2013b). The Jintan granite is U-rich and uranium mineralization has been discovered in the pluton (Zhao et al., 2013b). Therefore, it is an excellent location to investigate the relationship between biotite and muscovite-bearing granites, as well as to understand the mechanism of U enrichment in the Triassic granites of South China. This paper presents a study of zircon U—Pb ages and Hf isotopes, whole-rockmajor-trace elements and Sr—Nd isotopes from the Jintan pluton and major element analyses of biotites and muscovites in the biotite and muscovite-bearing phases. The aim of the study is to (1)better constrain the petrogenesis of Jintan pluton; (2)explore the relationship between biotite granite and two-mica granites in the Jintan pluton; (3)provide important insights into the mechanism of U enrichments in the Triassic granites of South China.

2. Geological setting and samples

The South China Block (SCB) consists of the Yangtze Block in the northwest and the Cathaysia Block in the southeast (Fig. 1. Li et al., 2012; Jiang et al., 2015). The two blocks amalgamated along the Jiangshan-Shaoxing Fault (JSF) in the early to middle Neoproterozoic (Li et al., 2008, 2009). The Cathaysia Block consists of a Proterozoic basement and a Sinian-Mesozoic sedimentary and volcanic cover (Chen and Jahn, 1998). The Yangtze Block consists of late Archean to Proterozoic basement and Cambrian to Triassic marine sedimentary rocks and a cover of Jurassic-Cretaceous and Cenozoic continental sedimentary rocks (Chen and Jahn, 1998; Hu et al., 2017). The SCB was tectonically active at different times in the Neoproterozoic, Early Paleozoic, and Mesozoic according to sedimentary, metamorphic and magmatic records (Li, 1998). Granites emplaced during these periods are widely distributed in South China, which makes the SCB one of the world's rare examples of a large granite province dominated by Mesozoic (including Triassic, Jurassic and Cretaceous) magma activity (Wang et al., 2013; Zhou et al., 2006). Extensive exposures of intrusive and extrusive rocks and related deposits (such as W, Sn, U,*etc.*) occur throughout the SCB(Hu et al., 2017).

The Jintan pluton is located geographically to the west of Xiajiang County in the Central Jiangxi Province of South China and geologically within the eastern Wugongshan tectonic belt. It crops out as an elliptical shape with an outcrop area of 164 km^2 (JGS, 1984) and a northwestern axial direction and intruded into Sinian to Cambrian metasedimentary sequences (Fig. 2). The Jintan pluton is predominantly composed of medium- to coarse-grained biotite granite, with some medium grained two-mica granites intruded into the biotite granite and crops out as stocks in the east, southwest and northwest of the pluton (Fig. 2). Restites and microgranular enclaves are not observed in the Jintan pluton. As reported by Zhao et al. (2013b), the two-mica granite in the east of the pluton formed at ~239 Ma with equigranular texture and massive structure and contains a few garnets. But the two-mica granite located in the southwest and northwest of the pluton has not been studied before. Our present study focuses on the biotite granite and two-mica granite in the southwest and northwest parts of the pluton. The biotite granite is porphyritic textured with megacrysts of K-feldspar. The main mineral constituents include K-feldspar (30–35%), plagioclase (25–30%), quartz (30–35%) and biotite (8–10%), with accessory apatite, zircon, monazite, magnetite and ilmenite (Fig. 3). The two-mica granite in the southwest and northwest of the pluton has medium-grained or porphyritic texture with phenocrysts of K-feldspar. It consists primarily of K-feldspar (30–35%), plagioclase (20–25%), quartz (35–40%), biotite (3–5%) and muscovite (1–2%), but lacks garnet, and contains accessory apatite, monazite and zircon (Fig. 3). Therefore, as mentioned above, the rocks in Jintan pluton can be classified into three types of granite: (1)biotite granite (BG) which is the main lithology of the pluton, (2)two-mica granite (TMG) which located in the southwest and northwest part of the pluton, and (3)garnet-bearingtwo-mica granite (GTMG) which is located in the eastern part of the pluton (Fig. 2). Some uranium deposits have been discovered in the GTMG(Zhao et al., 2013b), but none have yet been found in the BG or TMG.

3. Analytical methods

Zircons were separated using conventional heavy liquid and magnetic techniques and purified by the handpicking under a binocular microscope, and then cast into an epoxy mount. The mount was then polished to expose the grain centers and carbon-coated. The internal structures of the zircons were examined using cathodoluminescence (CL) images prior to U—Pb isotopic analysis. Sample 08JX04–1,08JX05–1, 08JX07–1 zircon U—Pb dating were made at the Guangzhou Institute of Geochemistry, Chinese Academy of Sciences (GIG-CAS), and sample 14JX08–1 zircon U—Pb dating were done at School of Resources and Environmental Engineering, Hefei University of Technology. All Zircon U—Pb analyses were performed using an Agilent 7500a ICP-MS, equipped with a RESOlution M-50laser-ablation system. Spot sizes of 32 μm with a laser frequency of 8 Hz were used. U–Th–Pb ratios and U concentrations were determined relative to TEMORA zircons (Black et al., 2003) and the standard NIST610 (Pearce et al., 1997), respectively. Raw count rates were measured for ^{29}Si, ^{204}Pb, ^{206}Pb, ^{207}Pb, ^{208}Pb, ^{232}Th and ^{238}U, and then calculated using the ICP-MS DataCal 6.7 (Liu et al., 2008). The detailed analytical techniques are described in Tu et al. (2011).

In situ zircon Hf isotopic analyses were carried out on the dated sites using a Neptune MC-ICPMS, equipped with a 193 nm laser, at the Guangzhou Institute of Geochemistry, Chinese Academy of Sciences (GIG-CAS). The detailed description of the two instruments can be found in Zhang et al. (2014). Spot sizes of 44 μm with a laser repetition rate of 8 Hz and energy density of 5 J/cm^2 were used to obtain a signal intensity of ~ 5 V at ^{180}Hf mass. The detailed analytical technique and data correction procedures are described in Wu et al. (2006). The mean β_{Yb}($^{172}Yb/^{173}Yb$) value obtained from zircon itself was applied for the interference correction of ^{176}Yb and ^{176}Lu on ^{176}Hf (Wu et al.,

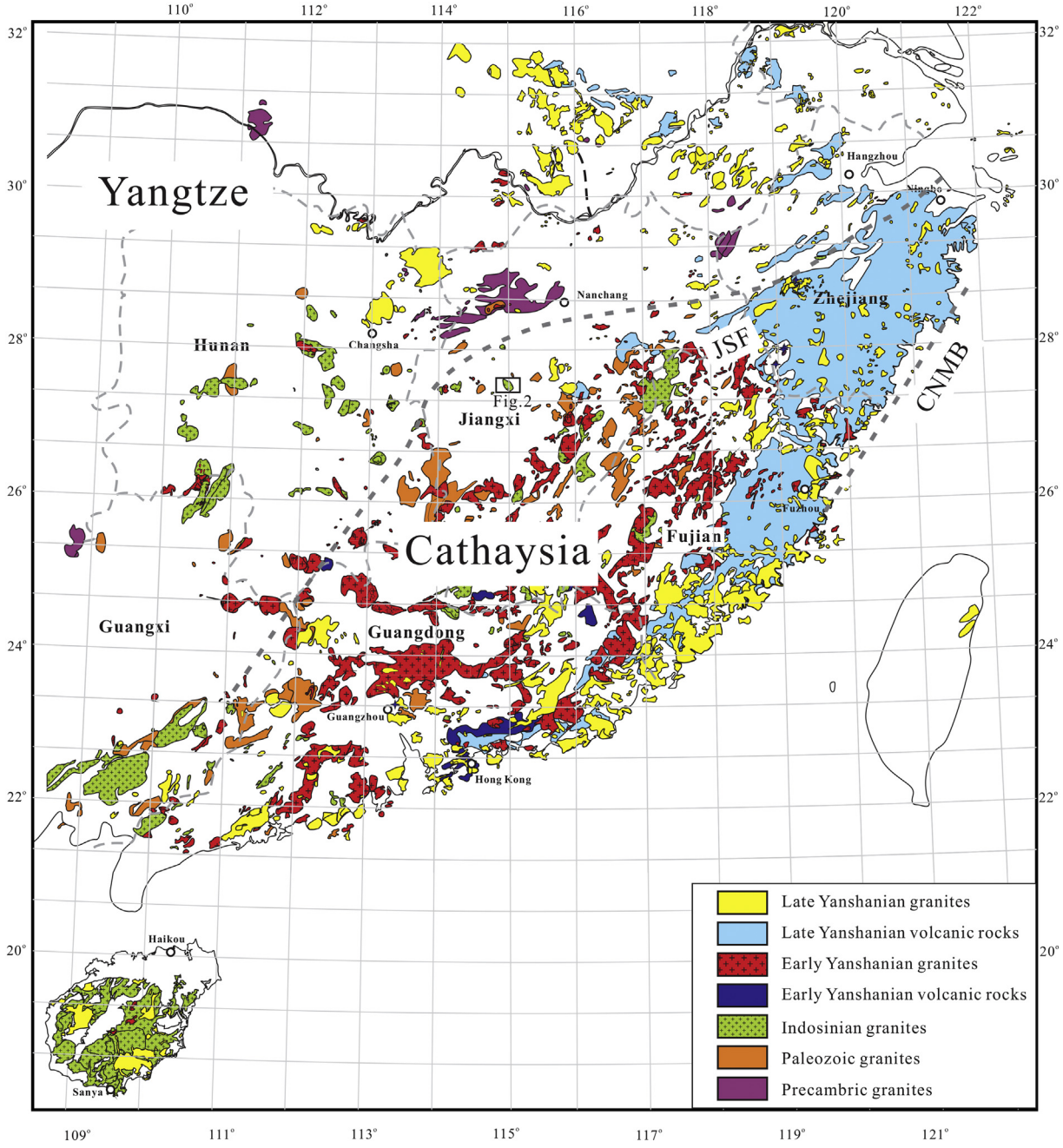

Fig. 1. Distribution of Mesozoic igneous rocks in southeastern China (modified after Li et al., 2012; Jiang et al., 2015). JSF, Jiangshan-Shaoxing Fault; CNMB, Changle-Nan'ao Metamorphic Belt.

2006). The ratios $^{176}Yb/^{172}Yb = 0.5886$ and $^{176}Lu/^{175}Lu = 0.02655$ were used for the elemental fractionation correction. Due to the extremely low $^{176}Lu/^{177}Hf$ in zircon (normally <0.002 in the studied samples), the isobaric interference of ^{176}Lu on ^{176}Hf is negligible (Kinny and Maas, 2003). No relationship between $^{176}Yb/^{177}Hf$ and $^{176}Hf/^{177}Hf$ ratios was observed in the studied samples, indicating that the correction of ^{176}Yb interference on ^{176}Hf is precise for obtaining accurate $^{176}Hf/^{177}Hf$ values. During analysis of the unknown samples, the zircon standard (GJ-1) and Mud Tank gave $^{176}Hf/^{177}Hf$ ratios of 0.282002 ± 25 (2σ; $n = 9$) and 0.252496 ± 18 (2σ; n = 9), respectively, which are identical with the preferred mean values measured using the LA-MC-ICPMS method (Gerdes and Zeh, 2006; Woodhead et al., 2004). The uncertainties of calibrated isotope ratios, including those from the sample, standards, and reference values, are given at ±2σ. The measured $^{176}Lu/^{177}Hf$ ratios and the ^{176}Lu decay constant of 1.865×10^{-11} yr^{-1} (Scherer et al., 2001) were used to calculate initial $^{176}Hf/^{177}Hf$ ratios. The chondritic values of $^{176}Hf/^{177}Hf = 0.0332$ and $^{176}Lu/^{177}Hf = 0.282772$ (Blichert-Toft and Albarède, 1997) were used for the calculation of ε_{Hf} values.

Whole rock geochemical and Sr—Nd isotopic analyses were carried out at the GIG-CAS. Major element oxides were analyzed using a Rigaku RIX 2000 X-ray fluorescence spectrometer (XRF), and analytical uncertainties are mostly between 1% and 5% (Li et al., 2006). Trace elements were obtained by inductively coupled plasma-mass spectrometry (ICP-MS) after acid digestion of samples in high-pressure Teflon vessels, and detailed procedures are same as those described by Li et al. (2006). The USGS and Chinese National standards AGV-2, GSR-1, GSR-2, MRG-1, BCR-1, W-2 and G-2 were chosen for calibrating element concentrations of the analyzed samples. Analytical precision of REE and other incompatible element analyses is typically 1–5%. Sr and Nd isotopic ratios

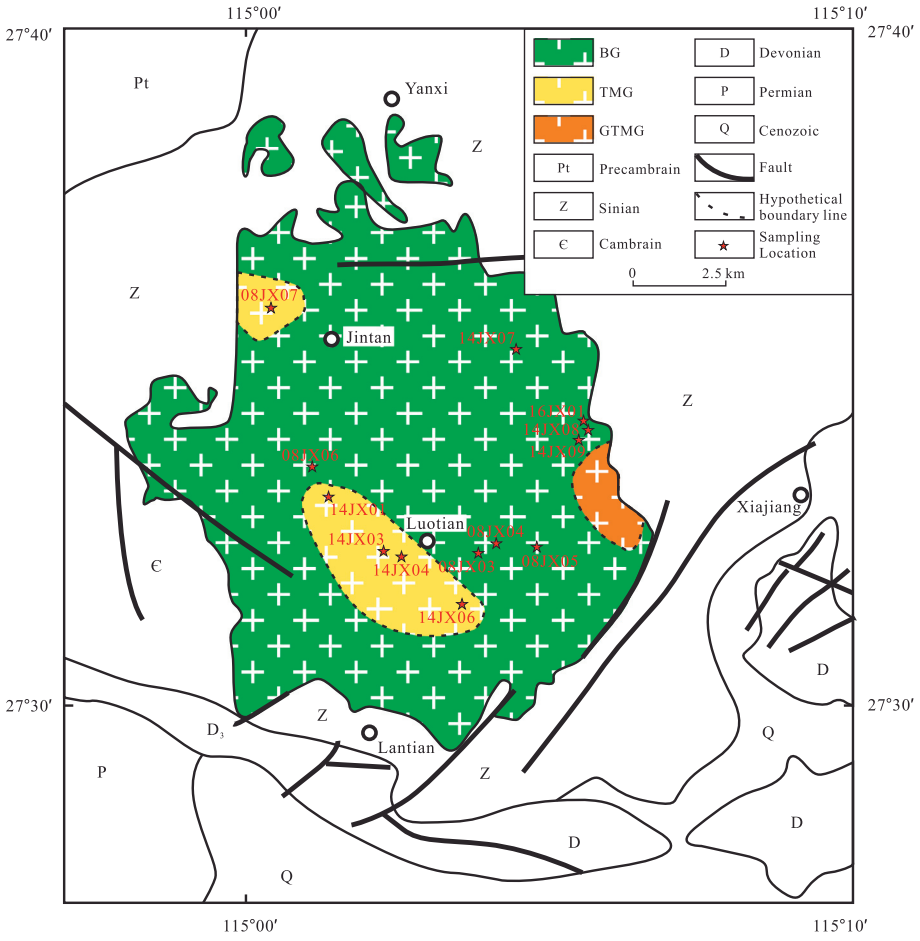

Fig. 2. Geological sketch map of the Jintan pluton showing sample locations (modified from the Jiangxi Bureau of Geology and Mineral Resources, 1984; Zhao et al., 2013b).

were measured on a subset of whole-rock samples using a Micro mass Isoprobe multicollector ICP-MS (MC-ICP-MS). Detailed procedures of sample preparation and chemical separation are the same as those described by Liang et al. (2003) and Wei et al. (2002). The procedure blanks were in the range of 200–500 pg for Sr and ≤ 50 pg for Nd. REEs were separated using the cation exchange columns, and the Nd fractions were further separated by HDEHP-coated Kef columns. Measured $^{143}Nd/^{144}Nd$ ratios were normalized to $^{146}Nd/^{144}Nd = 0.7219$. Reference standards were analyzed along with samples and gave $^{87}Sr/^{86}Sr = 0.710273 \pm 18$ (2σ) for NBS987 and $^{143}Nd/^{144}Nd = 0.512094 \pm 11$ (2σ) for Shin Etsu JNdi-1, which are comparable to the recommended values of NBS987 ($^{87}Sr/^{86}Sr = 0.710248$; McArthur, 1994) and Shin Etsu JNdi-1($^{143}Nd/^{144}Nd = 0.512115 \pm 7$; Tanaka et al., 2000).

Mineral compositions were obtained using the electron probe micro-analysis (EPMA) technique (*i.e.*, JEOLJXA-8100 Superprobe) at GIG-CAS. The operating conditions were: 15 kV accelerating voltage, 20 nA beam current, 5 μm beam diameter for mica and 1 μm for zircon,

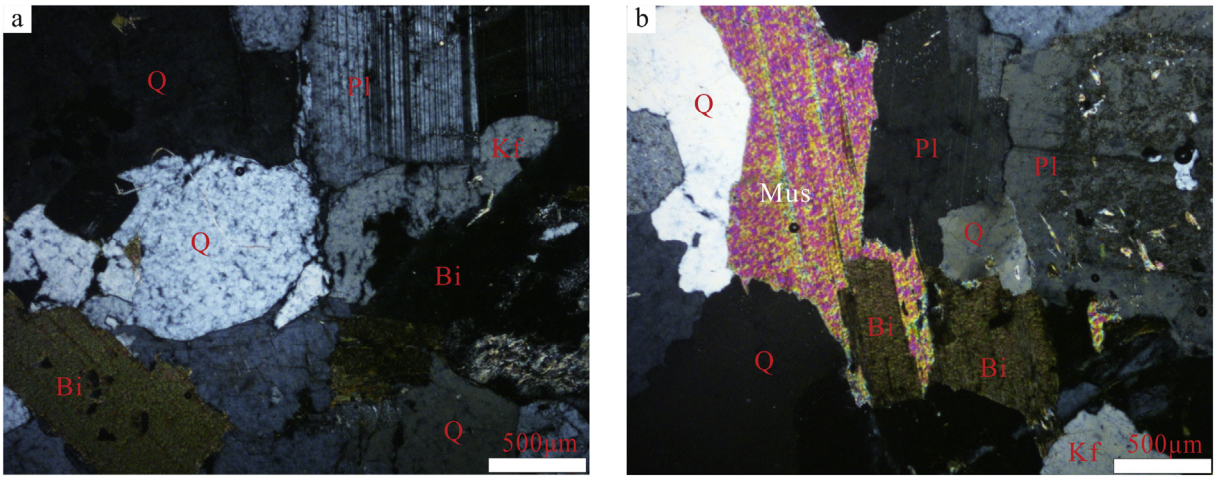

Fig. 3. Photomicrographs of rocks in the Jintan pluton. (a)biotite granite; (b)two-mica granite. Q = quartz, Bi = biotite, Pl = plagioclase, Kf = K-feldspar, Mus = muscovite.

and ZAF correction procedure for data reduction. The crystals of Wavelength Dispersive X-rays Spectrometers (WDS) are as the following: TAP (Si, Mg, Rb, Al, Na, Hf), LIF (Fe, Mn, Ti), LDE1 (F), and PETH (K, Cs, Ca, P, U, Th, Zr, Y). A variable peak counting time of 7–60 s was used, depending on the intensity of characteristic X-ray line and desired precision. The detection limits for all elements are lower than 300 ppm, depending on the element concentrations. For micas, the following natural and synthetic standards were used: Orthoclase (Si, K), pollucite (Rb, Cs), apatite (F, P), magnetite (Fe), tugtupite (Na, Cl), rhodonite (Mn), kaersutite (Ti) and pyrope garnet (Mg, Al, Ca). Chemical formulae of micas were calculated based on 24 anions (O, F, OH), and Fe^{3+} was calculated after the method by Lin and Peng (1994).

4. Results

4.1. Chemical characteristics of biotite and muscovite

The biotite and muscovite compositions of the granite samples from the BG and TMG are listed in Supplemental Table1 and Supplemental Table2, respectively.

The $Fe^{2+}/(Fe^{2+}+Mg)$ values of biotite vary from 0.51 to 0.61 for the TMG and from 0.43 to 0.52 for BG. The narrow range of biotite $Fe^{2+}/(Fe^{2+}+Mg)$ ratios rule out the possibility of modification by late-stage fluids (Chen et al., 2012 and references therein). Biotites from the TMG are characterized by higher Ti, Al, and Mn, and lower Mg compared to those from BG. On the Mg–(Al^{VI} + Fe^{3+} +Ti)–(Fe^{2+} +Mn) ternary diagram (Fig. 4), most biotites from the two granite types plot in the siderophyllite field. Those from BG plot closer to the eastonite field than those from the TMG.

Representative euhedral muscovites in the TMG were selected for analysis. The results reveal that they have TiO_2 contents higher than 0.4 wt% with a range from 0.46 wt% to 0.87 wt%. The muscovites have high Al_2O_3 (32.20–34.71 wt%) and Na_2O (0.38–0.74 wt%), but low FeO_T + MgO (4.16–5.77 wt%) and MnO (<0.06 wt%). They have compositions similar to high TiO_2 muscovite reported by Miller (1981) and can be regarded as primary muscovites, based on the Ti-Mg-Na ternary diagram (Fig. 5).

4.2. Zircon U—Pb dating

Three BG samples (08JX04–1, 08JX05–1 and 14JX08–1) and one TMG sample (08JX07–1) were selected for zircon U—Pb dating (Supplemental Table 3). Zircon grains from all four samples exhibit similar morphologies. They are all euhedral prismatic grains and mostly 100-350 μm in length with length/width ratios of ~1:1 to 3.5:1 and CL images show strong oscillatory zoning, implying a magmatic origin (Hoskin and Schaltegger, 2003). The age calculations and plotting of concordia diagrams were performed using Isoplot v. 3.23 (Ludwig, 2003).

4.2.1. Biotite granite

Sample 08JX04–1(location: N27°32′18″, E115°04′03″) is a fresh sample of medium-grainedBG, a total of 17 spot analyses of seventeen zircon grains were performed for it. As illustrated in Fig. 6, the U—Pb isotope data from seventeen spots are concordant within the analytical errors. Their U and Th contents vary from 129 ppm to 888 ppm and from 118 ppm to 265 ppm, respectively, with Th/U ratios varying from 0.16 to 1.01. Their $^{206}Pb/^{238}U$ ages vary from 217.3 Ma to 227.5 Ma, producing a weighted average age of 220.6 ± 2.1 Ma ($n = 17$, MSWD= 0.35) (Fig. 6), which can be regarded as the emplacement age of the BG.

Sample 08JX05–1(location: N27°32′07″, E115°04′54″) is a fresh sample of coarse-grainedBG from which a total of 18 spot analyses of eighteen zircon grains were obtained. The U and Th contents vary from 159 ppm to 1569 ppm and from 63 ppm to 925 ppm, respectively, with Th/U ratios from 0.09 to 2.33. One inherited or captured zircon grain exhibited a Meso-proterozoic age (08JX05–1-05). This analysis was omitted when calculating the crystallization age of this sample. The remaining 17 spots have $^{206}Pb/^{238}U$ ages ranging from 214.5 Mato 225.4 Ma, producing a weighted average age of 219.8 ± 2.4 Ma (n = 17, MSWD = 0.51) (Fig. 6), which is consistent with the results of sample 08JX04–1, within the analytical errors.

Sample 14JX08–1(location: N27°33′59.12″, E115°05′59.20″) is also a fresh sample of coarse-grainedBG, a total of 22 spot analyses on twenty-two zircon grains were undertaken. The U and Th contents vary from 152 ppm to 1155 ppm and from 84 ppm to 187 ppm, respectively, with Th/U ratios from 0.10 to 0.92. Their $^{206}Pb/^{238}U$ age range from216.3 Ma to 226.9 Ma, producing a weighted average age of 220.6 ± 1.3 Ma ($n = 22$, MSWD = 1.4) (Fig. 6), which is consistent with the results of samples 08JX04–1 and 08JX05–1 within the analytical errors.

4.2.2. Two-mica granite

Sample 08JX07–1(location: N27°35′54″, E115°00′30″) is a fresh sample of TMG, a total of 12 spot analyses were conducted on twelve zircon grains. The results show U and Th contents in the range of 237 ppm to 4601 ppm and from 159 ppm to 1893 ppm, respectively, with Th/U ratios from 0.13 to 2.22. One inherited or captured zircon grain exhibited a Late Paleozoic age (266 ± 7 Ma for 08JX07–1-03). The

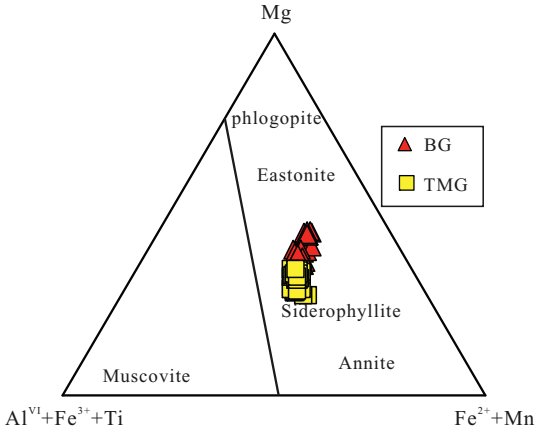

Fig. 4. Mg–(Al^{VI} + Fe^{3+} +Ti)–(Fe^{2+} +Mn) ternary diagram of biotite (after Foster, 1960).

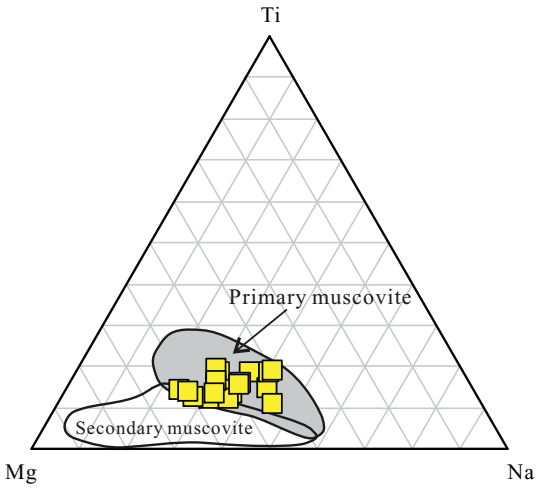

Fig. 5. Compositions of muscovites from TMG in terms of Ti, Mg and Na (atomic proportions). Fields of primary muscovite and secondary muscovite are after Miller etal. (1981).

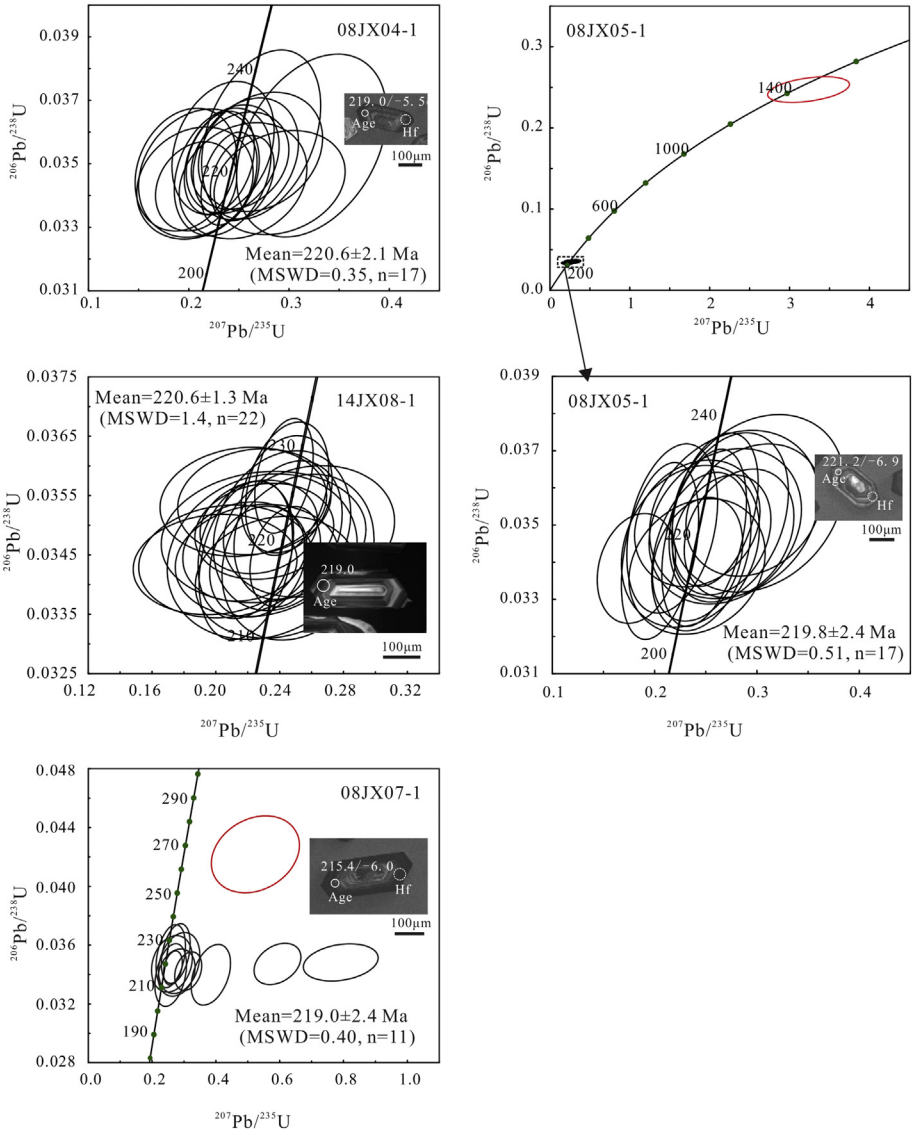

Fig. 6. LA–ICPMS zircon U—Pb condordia diagrams and weighted mean $^{206}Pb/^{238}U$ for the BG(08JX04–1, 08JX05–1 and 14JX08–1) and TMG (08JX07–1) from Jintan pluton. The red circles in sample 08JX05–1 and 08JX07–1 were excluded from the crystallization age calculations. Inset pictures show typical zircon grains in CL images with U—Pb and Hf analytical sites and results indicated.

remaining 11 spots have indistinguishable $^{206}Pb/^{238}U$ ages, within the analytical errors, ranging from 215 Ma to 224 Ma, producing a weighted average age of 219.0 ± 2.4 Ma ($n = 11$, MSWD = 0.40) (Fig. 6), which can be regarded as the crystallization age of TMG.

4.3. Whole-rock major and trace element data

The whole rock major and trace element data of the rocks in the Jintan pluton are presented in Supplemental Table 4; previously reported data of GTMG from Zhao et al. (2013b) are also included for comparison. Zircon saturation temperature was estimated using the thermometer given by Miller et al. (2003).

All of the BG,TMG and GTMG samples fall into the granite field and along the subalkalic trend on the total alkalis *versus* SiO_2 diagram (Fig. 7). BG has K_2O/Na_2O ratios of 1.34–1.89, showing weakly peraluminous to strongly peraluminous character with A/CNK ratios from 1.05 to 1.15 (Fig. 7). The TMG has K_2O/Na_2O ratios of 0.90–1.86 and exhibits strongly peraluminous features with A/CNK ratios from 1.13 to 1.24, while the GTMG has K_2O/Na_2O ratios of 1.33–1.67 with A/CNK ratios vary from 1.20 to 1.33 (except sample 09XJ-1, which has exceptionally high K_2O/Na_2O ratios of 3.43 and A/CNK ratios of 1.47 due to alteration as reflected by its high L.O·I value). BG and TMG have different evolutionary trends but the TMG and GTMG have trends that are similar to some extent on Harker diagrams (Fig. 8). With increasing SiO_2 for the BG, the Al_2O_3, TiO_2, Fe_2O_3, MgO and CaO contents decrease, whereas Na_2O, K_2O and P_2O_5 remains relatively constant, while the Al_2O_3, TiO_2, Fe_2O_3, MgO, CaO, Na_2O, K_2O and P_2O_5 are variable and scatter with increasing SiO_2 contents for the TMG. All samples fall into the high-Kcalc-alkaline series field (Fig. 8g).

The BG have higher Zr, Sr, Ba and Eu contents but lower U contents than the TMG. The elements Sr, Ba and Eu are clearly negatively correlated with SiO_2 for the BG but for the TMG these elements display significant variation over a narrow range of SiO_2 contents (Fig. 8j, k, l). The BG have higher overall Sr/Y ratios and La/Yb ratios compared to the TMG(Fig. 8o). On the primitive mantle-normalized trace element spider diagram (Fig. 9a), all samples exhibit significant negative anomalies of Ba, Nb, Sr and Ti and positive anomalies of Rb, Th, U and Pb. The difference is that TMG shows similar feature with BG, but the GTMG have more negative anomalies and more positive anomalies than BG (Fig. 9a). All of the BG,TMG and GTMG samples have generally consistent Chondrite-normalizedREE patterns (Fig. 9b), with enrichment in light rare earth elements (LREEs) (Fig. 9b). BG have $(La/Yb)_N$ ratios of

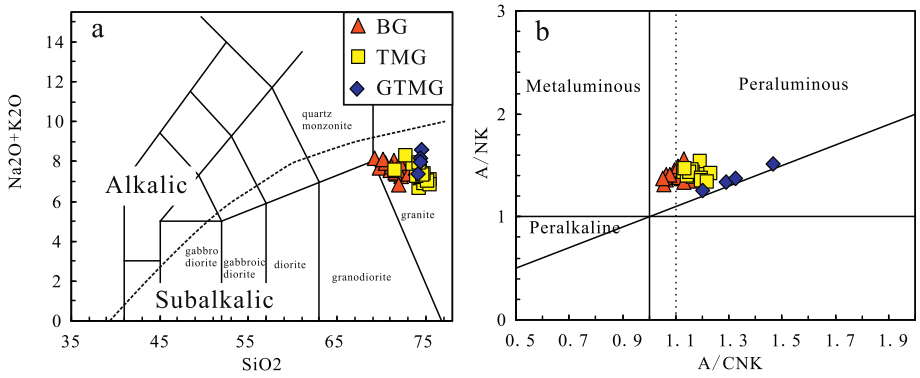

Fig. 7. Chemical classification of rocks in the Jintan pluton. (a)Total alkalis *vs* silica diagram (Middlemost, 1994); (b)A/NK *vs* A/CNK diagram (Maniar and Piccoli, 1989).

8.5 to 17.8. Compared with BG,TMG and GTMG have relatively low contents of LREEs and more variable contents of HREEs with $(La/Yb)_N$ ratios of 5.3 to 11.7 and 3.2 to 6.5, respectively. BG show moderately negative Eu anomaly with $Eu/Eu^* = 0.27–0.59$, and TMG and GTMG shows stronger negative Eu anomaly than BG with $Eu/Eu^* = 0.25–0.37$ and $Eu/Eu^* = 0.20–0.24$, respectively.

4.4. Whole-rock Sr—Nd isotopes

The results of Sr—Nd isotopes are presented in Supplemental Table 5. The BG has $^{87}Rb/^{86}Sr$ ratios (3.52 to 7.61) and $^{87}Sr/^{86}Sr$ ratios (0.722833 to 0.735200). Calculated $(^{87}Sr/^{86}Sr)_i$ vary from 0.711389 to 0.714225. The samples have $^{147}Sm/^{144}Nd$ ratios of 0.1037–0.1146 and $^{143}Nd/^{144}Nd$ ratios of 0.512004 to 0.512051. The $\varepsilon_{Nd}(t)$values vary from −9.91 to −9.16. The two-stage Nd isotopic model ages vary from 1.74 to 1.80 Ga.

A TMG sample has high $^{87}Rb/^{86}Sr$ ratios of 6.83 and $^{87}Sr/^{86}Sr$ ratios of 0.733211. Calculated $(^{87}Sr/^{86}Sr)_i$ is 0.711832. The sample has a $^{147}Sm/^{144}Nd$ ratio of 0.1171 and $^{143}Nd/^{144}Nd$ ratio of 0.512010. The $\varepsilon_{Nd}(t)$value is −10.02 with two-stage Nd isotopic model age of 1.81 Ga.

4.5. In-situ zircon Hf isotopes

Two dated BG samples (08JX04–1, 08JX05–1) and one dated TMG sample (08JX07–1) were analyzed for zircon Hf isotopes. Most analyses were conducted on the dated zircons, and the results are listed in Supplemental Table 6.

Zircons from the sample 08JX04–1 yield $\varepsilon_{Hf}(t)$values of −8.7 to −4.1, with two-stage Hf model ages (T_{DM2}) of 1518–1809 Ma. The zircons from the sample 08JX05–1 exhibit $\varepsilon_{Hf}(t)$values of −8.5 to −3.8 and Paleoproterozoic T_{DM2} ages of 1496–1795 Ma. The zircons $\varepsilon_{Hf}(t)$ values of sample 08JX07–1 ranges from −6.4 to −1.1, corresponding to T_{DM2} ages of 1327–1662 Ma.

5. Discussion

5.1. Geochronology of the Jintan pluton

The BG in the Jintan pluton were previously considered to have been intruded between ~250 Ma and ~ 257 Ma on the basis of biotite K—Ar dating (JGS, 1984), but Luo et al. (2010) and Zhao et al. (2013b) dated the intrusive phase using LA-ICPMS zircon U—Pb dating and obtained ages of 222.1 ± 1.6 Ma and 226 ± 2 Ma, respectively. The GTMG in the Jintan pluton gave an age of 239 ± 1 Ma, based on LA-ICPMS zircon U—Pb dating (Zhao et al., 2013b). The age of TMG in the Jintan pluton had not been constrained previously but were required to establish the unit's possible genetic relationship to the BG.

The results of our LA-ICPMS zircon U—Pb dating indicate that both BG and TMG formed at ~220 Ma. Since the external uncertainty of LA-ICPMS dating is about ±4% in 2SD (Klötzli et al., 2009; Li et al., 2015), the analytical results for the Triassic Jintan granite samples have an external uncertainty of about ±9 Ma (2SE). Therefore, new dating results for the Jintan BG are indistinguishable from zircon U—Pb ages of Luo et al. (2010) and Zhao et al. (2013b). As a consequence, it is evident that there are two stages of intrusions in the Jintan pluton. The GTMG formed in the Early Triassic period (~239 Ma, Zhao et al., 2013b), while the BG and TMG formed during the Late Triassic period (~220Ma).

5.2. Petrogenetic type: S-type or I-type?

Granites have commonly been divided into I-, S-, M- and A-types according to the nature of their protolith and their petrographical and geochemical features (Chappell, 1999; Whalen, 1985). Both BG and TMG in the Jintan pluton have negative whole-rock $\varepsilon_{Nd}(t)$and zircon $\varepsilon_{Hf}(t)$values, and contain some inherited zircons (Fig. 6), therefore they cannot belong to the M-type granite which formed from juvenile mantle-derived materials (Whalen, 1985). The studied Jintan pluton granites lack alkali mafic minerals. Although some biotites do occur, they show euhedral and tabular textures (Fig. 3) and thus are not late-crystallized minerals, indicating the original melts were not anhydrous. They also have low Zr + Nb + Ce + Y contents (192 to 364 ppm for the BG, 191 to 297 ppm for the TMG). Those characteristics are not consistent with a classification as A-type granites.

Mineralogical and geochemical features are commonly used to distinguish I-type granite from S-type granite. S-type granites generally contain relatively abundant Al-rich minerals, such as cordierite, muscovite, garnet and tourmaline, while I-type granites generally contain amphibole (Li et al., 2007a, 2007b; Wu et al., 2007; Zhao et al., 2016). Most S-type granites are strongly peraluminous with A/CNK>1.1, whereas most I-type granites are met aluminous with A/CNK<1 (Chappell, 1999; Zhao et al., 2016). The TMG in the Jintan pluton are strongly peraluminous with A/CNK = 1.13 to 1.33 (Fig. 7) and contain abundant primary muscovites (Fig. 5), consistent with their peraluminous character (Huang et al., 2015; Miller, 1981). Thus, the TMG can unambiguously be assigned an S-type granite classification.

In the absence of characteristic minerals for either I- or S-type granites, the geochemical features of the BG become critical for their classification. As illustrated in the Fig. 10, on the plots of Y*vs* Rb and Th *vs* Rb, all of the Jintan granite samples plot on the S-type granite trend line, demonstrating S-type affinity. Moreover, given the close spatial association with the TMG, their similar ages (Figs.2, 6) and consistent Sr—Nd isotope signatures (Fig. 11), the two granite types must have similar magma sources. Therefore, the BG should also be classified as S-type granite.

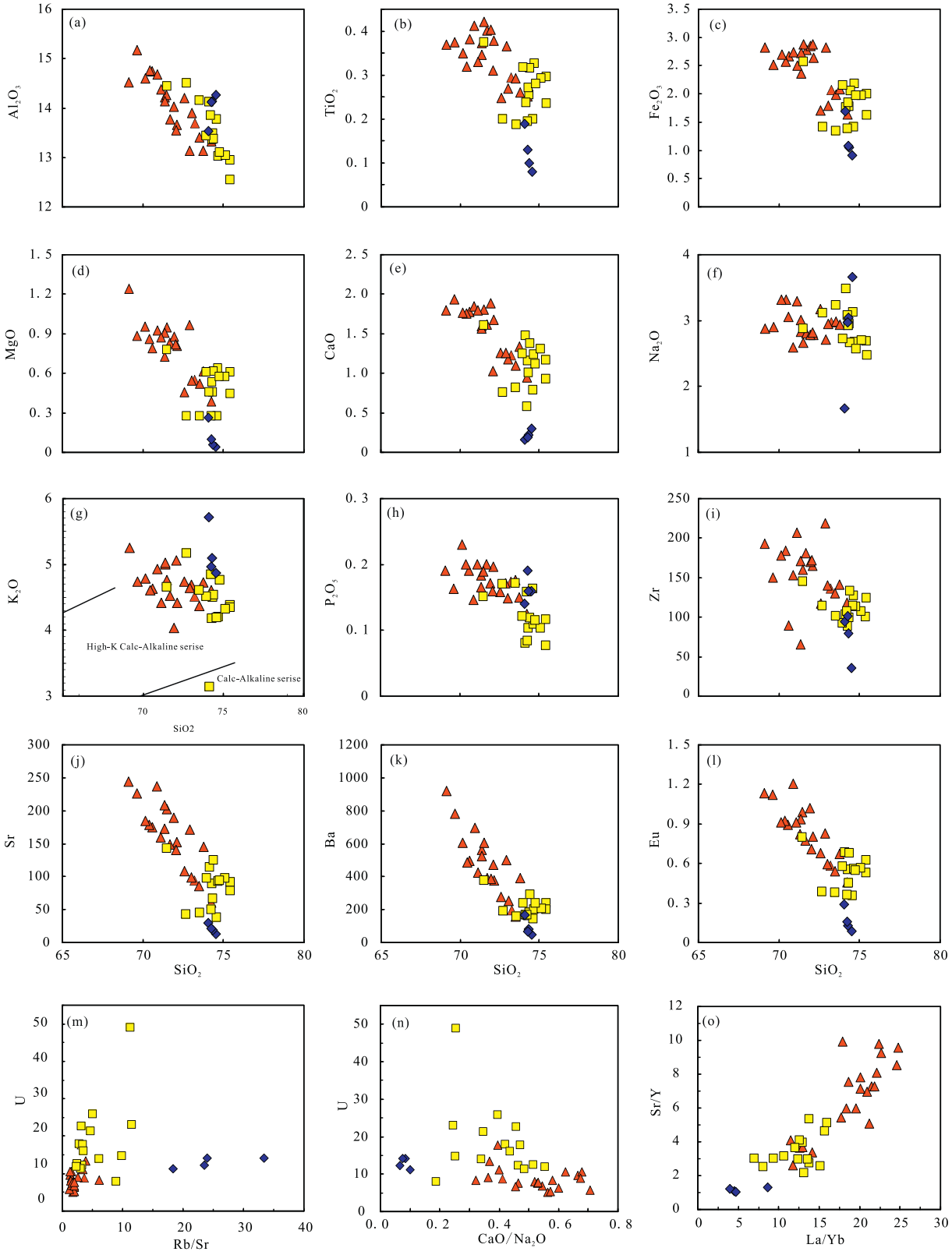

Fig. 8. Harker-type major and trace element plots for the Jintan granites. Symbols are the same as those in Fig. 7.

5.3. Sources of the granites

S-type granites are commonly considered to be derived from partial melting of supracrustal metasedimentary rocks (Sylvester, 1998). As discussed above, both BG and TMG in the Jintan granite are peraluminous (A/CNK>1) S-type granites. On a $\varepsilon_{Nd}(t)$*vs* t diagram, both the BG and TMG plot in the field of the parametamorphic basement of the Cathaysia Block (Fig. 11a). On the $\varepsilon_{Hf}(t)$*vs* t diagram (Fig. 12), all samples plot between the evolution lines of the upper and lower crust. They plot higher than the Luxi biotite granites and Xiazhuang

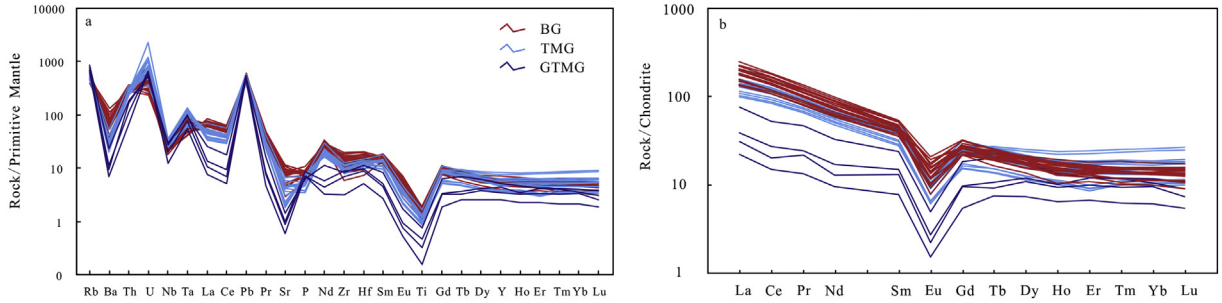

Fig. 9. (a)primitive mantle-normalized trace element spidergram and (b)chondrite-normalized REE diagram for the Jintan granite. Normalization values are from Sun and McDonough (1989).

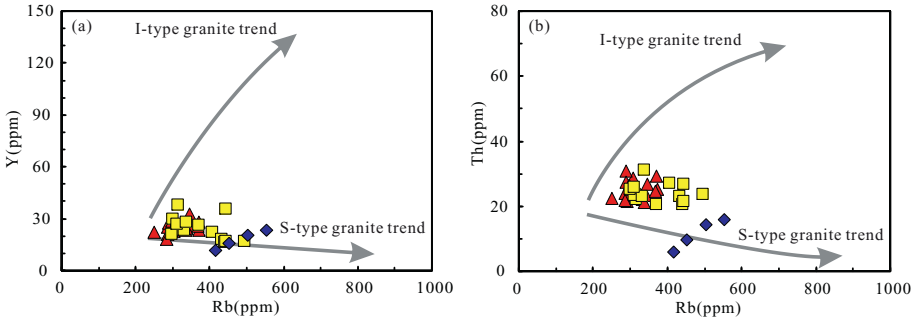

Fig. 10. Plots of Y(a)and Th (b)against Rb for the Jintan granites (after Li et al., 2007b). Symbols are the same as those in Fig. 7.

U-bearingtwo-mica granites in southern Jiangxi Province, suggesting that their parental magma lacked a significant mantle contribution (Chen et al., 2012) and were derived predominately from crustal materials that were probably different from the sources of the Luxi and Xiazhuang plutons. Specifically, the BG and TMG have Paleoproterozoic two-stage whole rock Nd isotopic model ages that are consistent with their two-stage zircon Hf isotopic model ages. All the above geochemical and isotopic data indicate that the Jintan granite formed through partial melting of metasedimentary crust.

The outcropping Mesoproterozoic basement represented by Zhoutan Group in central Jiangxi Province is mainly composed of schists, granulites and amphibolites (Zhao et al., 2011). It is suggested that the schists and granulites were of sedimentary origin, whereas the precursor to the amphibolites was basaltic (Hu and Zhang, 1998). The parametamorphic rocks in Central Jiangxi Province have Meso- to Palaeoproterozoic Nd isotopic model ages (Hu and Zhang, 1999; Zhao et al., 2011) and on the $\varepsilon_{Nd}(t)$*vs* t diagram (Fig. 11b), most Jintan pluton samples are similar to the Jurassic Daguzhai U-bearingtwo-mica granite, plotting in the range of parametamorphic rocks of the Mesoproterozoic Zhoutan Group. They are distinct from the Baimianshi U-richtwo-mica granite in Southern Jiangxi Province that is considered to be derived from the partial melting of the Taoxi Group (Dong et al., 2010), which is likely to also be the source of the Luxi and Xiazhuang granite in Southern Jiangxi Province. A source in the Zhoutan Group would also explain why the Jintan granites have higher $\varepsilon_{Hf}(t)$values than the Luxi and Xiazhuang granites in the southern Jiangxi Province (Fig. 12). As a result, we conclude that the Jintan granite is dominantly derived from

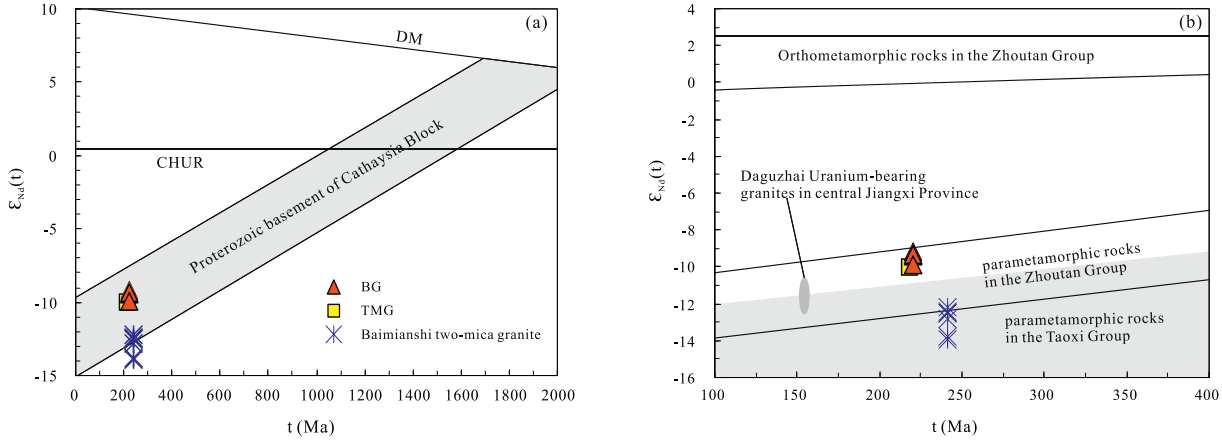

Fig. 11. Whole rock $\varepsilon_{Nd}(t)$ *vs* t diagrams of granites in Jintan pluton. Data of Proterozoic basement of Cathaysia Block are from Shen et al. (1993). Data of parametamorphic rocks in the Zhoutan Group are from Hu and Zhang (1998) and Hu and Zhang (1999). Data of orthometamorphic rocks in the Zhoutan Group are from Hu et al. (1999). Data of parametamorphic rocks in the Taoxi Group are from Shen et al. (2003). Data of Daguzhai Uranium-bearing granites and Baimianshi two-mica granite are from Zhao et al. (2011) and Dong et al. (2010), respectively.

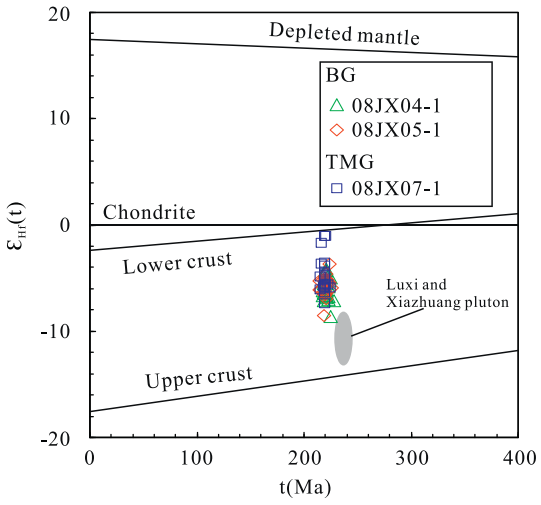

Fig. 12. Plot of t *vs.* zircon $\varepsilon_{Hf}(t)$values of the granites in Jintan pluton. The data of Luxi and Xiazhuang pluton come from Chen et al., 2012.

the partial melting of parametamorphic rocks of the Zhoutan Group. Limited partial melting of orthometamorphic rocks might also be involved as a few samples display higher $\varepsilon_{Nd}(t)$values than the range exhibited by the Zhoutan Group (Fig. 11b).

It is noteworthy that zircon $\varepsilon_{Hf}(t)$from the TMG extend to slightly higher values than those of the BG(Fig. 12) and that the BG and TMG exhibit different evolutionary trends on Harker diagrams (Fig. 8). These observations imply that the BG and TMG were derived from the partial melting of sediments with different characteristics. As illustrated in Fig. 13, the BG have relatively low Al_2O_3/TiO_2 ratios and high CaO/Na_2O ratios (>0.3), which is similar to the strongly peraluminous granites in the Lachlan Fold Belt (LFB) in southeastern Australia(Sylvester, 1998), indicating a derivation from partial melting of clay-poorpsammite-derived sources at high temperature (Jung and Pfander, 2007; Sylvester, 1998). In contrast, the TMG have large variations in Al_2O_3/TiO_2 ratios and CaO/Na_2O ratios, which is similar to the European Hercynides (Fig. 13, Sylvester, 1998). Their highly variable CaO/Na_2O ratios are similar to the Baimianshi U-richtwo-mica granites (Dong et al., 2010), Douzashan U-bearingtwo-mica granite (Zhao et al., 2016) and Xiazhuang U-bearingtwo-mica granite (Chen et al., 2012), all of which are regarded as Triassic partial melts of clay-rich pelitic rocks in South China(Chen et al., 2012; Dong et al., 2010; Zhao et al., 2016). The geochemical similarities therefore suggest that the Jintan TMG were also derived by partial melting of clay-rich pelitic rocks.

Biotite is an excellent indicator of the oxidation state of the parental magma from which it crystallized (Wones and Eugster, 1965). The $Fe^{2+}/(Fe^{2+} + Mg^{2+})$ ratio of the biotite trisoctahedron provides an index of the redox degree (Speer, 1984). In the BG, this ratio ranges from 0.51 to 0.61, which is distinctly higher than those of the TMG (0.43–0.52) and suggests that the two magmas had different oxygen fugacities. On the Fe^{2+}–Fe^{3+}–Mg ternary diagram (Fig. 14a), all samples lie above the NNO buffer, similar to the Luxi and Xiazhuang S-type granite (Chen et al., 2012). As shown in Fig. 14b, the $\log(fO_2)$ values are estimated to be −14.3 to −11.6 for the BG and from −15.8 to −12.8 for the TMG, respectively. The TMG magmatic system is more reduced than the BG magmatic system, indicating the greater involvement of clay-rich carbonaceous pelitic rocks in the origin of TMG than in the BG(Zhao et al., 2011, 2016).

5.4. Partial melting vs Fractional crystallization

As the TMG are spatially associated with coeval BG, it raises the possibility that the TMG are highly fractionated derivatives of the BG, resembling the coexisted biotite granites and two-mica granites of Mesozoic granitic plutons in South China reported by Jiang and Zhu (2017) and Chen et al. (2012). Based on this premise, the TMG should have absolutely higher SiO_2 than BG with little compositional overlap, and the linear covariation on TMG element plots should be observed (Chen et al., 2012; Garcia-Arias and Stevens, 2017; Jiang and Zhu, 2017). As illustrated in Fig. 8, however, the TMG display significant compositional overlap with the BG and compositional variations within the TMG do not form well-defined trends, which makes the fractional crystallization scenario much less plausible.

Elements such as Li, Be, B and F will concentrate in the final, interstitial liquid fractions in any crystallizing granitic system (Clemens and Stevens, 2012). The highest Rb/Sr ratio of TMG is up to 11.52, which could be an extremely fractional crystallization in this hypothesis. However, the lack of minerals such as tourmaline and beryl in the TMG likely implies that the TMG magmatic system was not rich in Li, Be and B. Additionally, the F contents of TMG biotites (0.335%–0.766%) overlap with those of BG biotites (0.395%–0.804%), indicating that the TMG and BG magmatic systems had similar F contents (Chen et al., 2012). This observation does not support the view that the TMG are highly fractionated products of the BG. In contrast, as the composition of source rocks exerts the first-order control on the composition of granitic melts in closed systems (Gao et al., 2016), the consistent F contents of biotites from the TMG and BG suggest that the source rocks of the two granite types

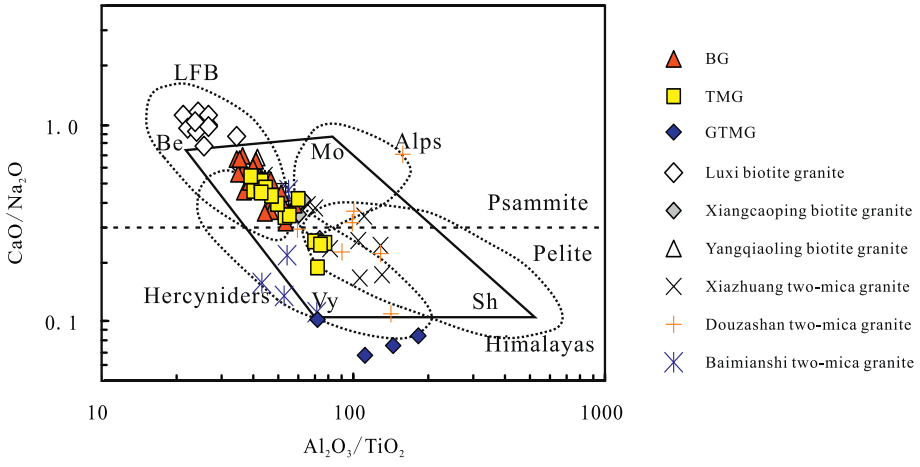

Fig. 13. Plot of Al_2O_3/TiO_2*vs.* CaO/Na_2O for the Jintan granites (after Sylvester, 1998). The data of Luxi biotite granite and Xiazhuang two-mica granite come from Chen et al., 2012; the data of Xiangcaoping biotite granite,Yangqiaoling biotite granite and Douzashan two-mica granite come from Zhao et al., 2016; the data of Baimianshi two-mica granite come from Dong et al., 2010

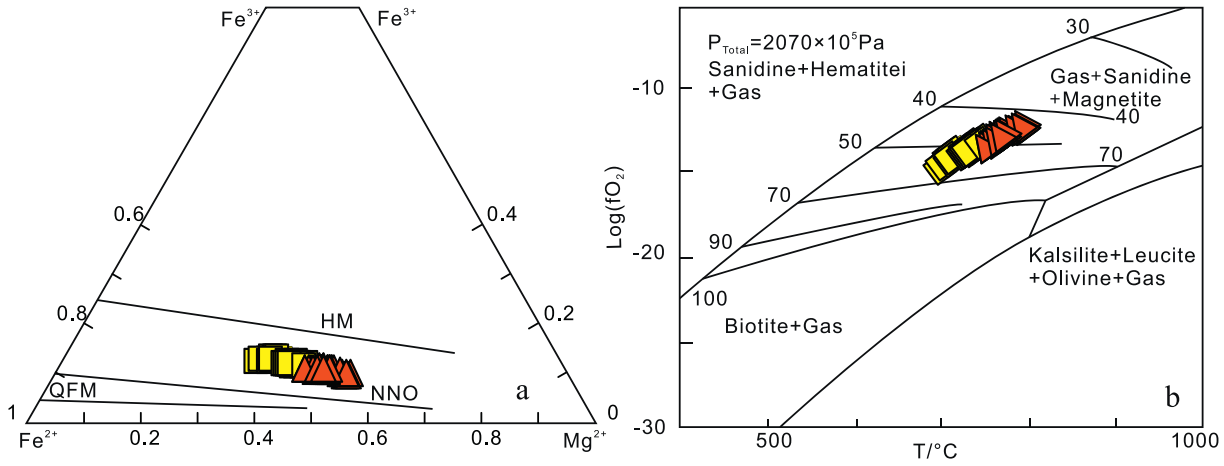

Fig. 14. (a)Mg^{2+}–Fe^{3+}–Fe^{2+} and (b)T–log(fO_2) diagrams for biotite of the Jintan granite (Wones and Eugster, 1965). QFM: Quartz–Fayalite–Magnetite buffer; NNO: Ni–NiO buffer; HM: Magnetite–Hematite buffer. Symbols are the same as those in Fig. 4.

had similar F contents. Alternatively, the compositional differences between the TMG and BG can be explained by partial melting of heterogeneous source rocks under differing conditions (Clemens and Stevens, 2012; Gao et al., 2016) and we prefer this scenario to account for the coeval TMG and BG in the Jintan pluton.

Notably, the TMG have whole-rock $\varepsilon_{Nd}(t)$values similar to the BG (Fig. 11), but higher zircon $\varepsilon_{Hf}(t)$values than the BG(Fig. 12). This Nd—Hf isotope decoupling, as in the case for the Douzashan two-mica granite and Xiangcaoping biotite granite (Zhao et al., 2016), further indicates that the TMG and BG were likely derived from similar sediments but under different melting conditions. In this scenario, the systematic differences in both major and trace elements between the BG and TMG(Figs.8, 9) relate to melting temperatures, and thus the extents of partial melting (Zhao et al., 2015). The magmatic temperature estimates obtained *via* zircon saturation thermometry (Miller et al., 2003) for the BG are in the range of 715 to 822 °C, distinctly higher than the 683 to 785 °C range obtained for the TMG and demonstrating that the extent of partial melting for the BG magma was higher than that of the TMG magma.

The La/Yb and Sr/Y ratio of intermediate-felsic magmatic rocks intrinsically reflect the mineral assemblages (plagioclase + garnet) in the magma source region (Chapman et al., 2015; Chiaradia, 2015; Profeta et al., 2015). Thus, these ratios can be regarded as broadly reflecting the variable depths of magma production (Tang et al., 2017). Both the BG and TMG lack heavy REE (HREE) and Y depletions (Fig. 9), implying garnet was absent in the sources. The BG have higher Sr/Y and La/Yb ratios (Fig. 8o) and greater MgO contents (Fig. 8d) than the TMG, indicating that the BG parental magmas were generated at deeper levels and from more mafic sources than the TMG. Thicker crust not only favours evolution of magmas at deeper average levels but also leads to a more extensive magmatic differentiation at those levels (Chiaradia, 2015). Such an interpretation is also consistent with the trends on Harker diagrams where the BG exhibit linear covariations signaling extensive fractional crystallization, whereas the TMG display scatter over generally more restricted element concentrations and pointing to a limited fractional crystallization (Fig. 8). The negative correlations between Sr, Ba, Eu and SiO_2 and negative anomalies of Ba, Nb, Sr and Ti for the BG imply some degree of fractionation of plagioclase and/or K-feldspar, biotite, Ti-bearing phases (such as ilmenite and titanite) and apatite (Li et al., 2007a), and the scatter of major elements and negative anomalies of Ba, Nb, Sr and Ti for the TMG are likely to mainly reflect minor heterogeneities in the original melts.

In summary, we conclude that both the BG and TMG were derived from the partial melting of parametamorphic rocks of the Mesoproterozoic Zhoutan Group in Central Jiangxi Province. BG was derived from relatively mafic, clay-poor psammite metasedimentary sources at deeper levels and higher temperatures and underwent extensive fractional crystallization, while TMG was derived from more felsic, clay-rich pelitic metasedimentary sources at higher levels and lower temperatures, followed by limited fractional crystallization.

6. Implication for the enrichment of U in granite

Previous exploration and scientific studies have indicated that granite-hosted uranium deposits in South China were closely related to U-rich granites (U>10 ppm; Zhang and Zhang, 1991). Those granites have been regarded as the uranium sources for later hydrothermal mineralization events (Chen, 2004; Chen et al., 2012; Hu et al., 2008; Zhang et al., 2017; Zhao et al., 2011, 2016). Although both the TMG and BG in the Jintan pluton formed at ~220 Ma, the TMG has relatively high U contents ranging from 7.85 ppm to 48.90 ppm with an average of 18.44 ppm whereas the BG shows relatively low U contents ranging from 4.99 ppm to 17.72 ppm with an average of 8.64 ppm (Supplemental Table 4). Interestingly, the U contents of the TMG are similar to that of the Douzashan uranium-bearing TMG (7.98–26.09 ppm with average 17.14 ppm, Zhao et al., 2016) and Xiazhuang uranium-bearing TMG (8.29–49.02 ppm with average 20.39 ppm, Chen et al., 2012).

Previous studies revealed that most of the Triassic U-rich granites contain muscovite and are strongly peraluminous S-types with metasedimentary sources. As discussed above, we suggest that the TMG and BG in Jintan pluton were likely derived from parametamorphic rocks of Zhoutan Group from slightly different sources and under different melting conditions. Previous studies indicated that parametamorphic rocks in the Zhoutan Group have relatively high U contents (Hu and Zhang, 1998; Zhao et al., 2011). Therefore, the fundamental question is: why are the TMGs rich in U, whereas BGs are not? Notably, the samples with low CaO/Na_2O ratios exhibit higher U contents (Fig. 8n), indicating source factors play an important role in the generation of the U-rich granites (Zhao et al., 2011, 2013b, 2016). The clay-rich carbonaceous metasedimentary sources of the TMG generally have high U contents, which was syngenetically deposited and absorbed onto organic material or clay minerals under anoxic conditions (Zhao et al., 2016). Therefore, lower degree partial melting of clay-rich carbonaceous pelitic rocks resulted in melts with extremely high U contents because the element usually behaves as an incompatible element in magmas (Hu et al., 2008). Substitution between U and other incompatible trace elements (such as Th, Zr, Ce and Y)bonded with O^{2-} could have promoted the formation of U-bearing accessory REE minerals, such as monazite, zircon and allanite. The TMG, however, have lower total and light REE contents than the BG(Fig. 9) and were generated from melts formed at lower temperatures in a more reduced environment and at lower pressure conditions. These physical-chemical

conditions inhibit the formation of U-bearing accessory REE minerals in the residual magma (Chen et al., 2012; Zhang et al., 2017; Zhao et al., 2016), hence, U is retained and enriched in the melts during the process of magma evolution.

It is suggested that fractional crystallization plays an important role in producing U-rich granites (Cuney, 2009), as documented in the Xiazhuang U-bearing granite (Chen et al., 2012). However, as illustrated in Fig. 8m, the U contents of the fractionated samples with higher Rb/Sr values are identical or a little higher than that of samples with lower Rb/Sr values, indicating fractional crystallization is not the main mechanism for enrichment of U in the TMG in Jintan pluton, and this observation is similar to that made for the Douzashan uranium-bearing granite (Zhao et al., 2016).

In summary, we argue that the combination of a U-rich source, physical-chemical conditions such as low partial melting temperature or low degree of partial melting, reduced conditions and the low REE and LREE contents of melts for the TMG in Jintan pluton favored a high U content for the magma system, thus resulting in U-rich granite. It is worth noting that the Early Triassic GTMG also has higher U content (11.14–14.11 ppm with average 12.87 ppm) than the BG(Zhao et al., 2013b) and that uranium ores occur as veins or lenses of pitchblende along and adjacent to the *E*-W striking faults within the GTMG in the east of the pluton (Zhao et al., 2013b). No significant uranium mineralization has been discovered in the Late Triassic TMG in the southwest and northwest of the pluton. We consider it possible that the later magmatism represented by the BG and TMG might be conducive to generating uranium mineralization in the GTMG, though confirming this supposition requires further investigation.

7. Conclusions

La-ICPMS zircon U—Pb dating results indicate that both BG and TMG in the Jintan pluton formed at ~220 Ma. Both can be classified as S-type granites and were likely derived from the partial melting of parametamorphic rocks in the Zhoutan Group. The BG had clay-poor psammite sources at deeper levels at relatively higher temperatures, and underwent an extensive fractional crystallization, while the TMG derived from the clay-rich pelitic rocks sources at relatively higher levels and lower temperatures accompanied by only limited fractional crystallization. We suggest that the combination of differing metasedimentary sources and physical-chemical conditions were responsible for the different U contents in the two types of granite.

Acknowledgements

We thank Linli Chen, Congying Li, Ying Liu, Xianglin Tu, Xirong Liang and Le Zhang for their assistance in EMPA,La-ICPMS zircon U—Pb dating, Whole rock geochemical and Sr—Nd isotope, and zircon Hf isotopes analyses. This work was supported by the National Natural Science Foundation of China (Grant 41303020, 41173039, 41763005), research grant of State Key Laboratory of Isotope Geochemistry, GIG-CAS (Grant SKLIG-KF-13-06), research grant of Fundamental Science on Radioactive Geology and Exploration Technology Laboratory, ECUT(RGET1803) and Chinese Scholarship Council (Grant CSC201608360054). We are grateful to the two anonymous reviewers for their careful constructive comments and the editor for guidance, which are greatly helpful for us to improve the paper.

Appendix A. Supplementary data

Supplementary data to this article can be found online at https://doi.org/10.1016/j.lithos.2018.09.003.

References

Black, L.P., Kamo, S.L., Allen, C.M., Aleinikoff, J.N., Davis, D.W., Korsch, R.J., Foudoulis, C., 2003. TEMORA 1: a new zircon standard for Phanerozoic U-Pb geochronology. Chem. Geol. 200, 155–170.
Blichert-Toft, J., Albarède, F., 1997. The Lu-Hf isotope geochemistry of chondrites and the evolution of the mantle-crust system. Earth Planet. Sci. Lett. 148 (1), 243–258.
Brown, M., 2013. Granite: from genesis to emplacement. Geol. Soc. Am. Bull. 125 (7–8), 1079–1113.
Chapman, J.B., Ducea, M.N., Decelles, P.G., Profeta, L., 2015. Tracking changes in crustal thickness during orogenic evolution with Sr/Y: an example from the north American Cordillera. Geology 43 (10), 919–922.
Chappell, B.W., 1999. Aluminium saturation in I- and S-type granites and the characterization of fractionated haplogranites. Lithos 46 (3), 535–551.
Chen, P.R., 2004. Geodynamic setting of Mesozoic magmatism and its relationship to uranium met allogenesis in southeastern China. Uranium Geology. 20 (5), 266–270 (in Chinese with English abstract).
Chen, J.F., Jahn, B.M., 1998. Crustal evolution of southeastern China: Nd and Sr isotopic evidence. Tectonophysics 284 (1–2), 101–133.
Chen, W.F., Chen, P.R., Huang, H.Y., Ding, X., Sun, T., 2007. Chronological and geochemical studies of granite and enclave in Baimashan pluton, Hunan, South China. Sci. China. Ser. D Earth Sci. 50 (11), 1606–1627.
Chen, Y.W., Bi, X.W., Hu, R.Z., Dong, S.H., 2012. Element geochemistry, mineralogy, geochronology and zircon Hf isotope of the Luxi and Xiazhuang granites in Guangdong province, China: Implications for U mineralization. Lithos 150 (0), 119–134.
Chiaradia, M., 2015. Crustal thickness control on Sr/Y signatures of recent arc magmas: an Earth scale perspective. Sci. Rep. 5, 8115.
Clemens, J.D., Stevens, G., 2012. What Controls Chemical Variation in Granitic Magmas? Lithos. 134–135(0). pp. 317–329.
Cuney, M., 2009. The extreme diversity of uranium deposits. Mineral. Deposita 44 (1), 3–9.
Dong, C.Y., Zhao, K.D., Jiang, S.Y., Chen, W.F., Chen, P.R., Ling, H.F., Yang, S.Y., 2010. Ziron geochronology, geochemistry and petrogenesisi of granite from Baimianshi uranium ore district in the Southern Jiangxi Province. Geol. J. China Univ. 16 (2), 149–160 (in Chinese with English abstract).
Foster, M.D., 1960. Interpretation of the composition of trioctahedral micas. U.S. Geological Surevery Professional Paper. 354, 11–49.
Gao, P., Zheng, Y.F., Zhao, Z.F., 2016. Experimental melts from crustal rocks: a lithochemical constraint on granite petrogenesis. Lithos 266-267, 133–157.
Gao, P., Zheng, Y.-F., Zhao, Z.-F., 2017. Triassic granites in South China: a geochemical perspective on their characteristics, petrogenesis, and tectonic significance. Earth Sci. Rev. 173, 266–294 Suppl. C.
Gao, P., Zheng, Y.-F., Chen, Y.-X., Zhao, Z.-F., Xia, X.-P., 2018. Relict zircon U-Pb age and O isotope evidence for reworking of Neoproterozoic crustal rocks in the origin of Triassic S-type granites in South China. Lithos 300-301, 261–277.
Garcia-Arias, M., Stevens, G., 2017. Phase equilibrium modelling of granite magma petrogenesis: B. an evaluation of the magma compositions that result from fractional crystallization. Lithos 277, 109–130.
Gerdes, A., Zeh, A., 2006. Combined U–Pb and Hf isotope LA-(MC-)ICP-MS analyses of detrital zircons: Comparison with SHRIMP and new constraints for the provenance and age of an Armorican metasediment in Central Germany. Earth Planet. Sci. Lett. 249 (1), 47–61.
Hoskin, P.W.O., Schaltegger, U., 2003. The composition of zircon and igneous and metamorphic petrogenesis. Rev. Mineral. Geochem. 53 (1), 27–62.
Hu, G.R., Zhang, B.T., 1998. Geochemical study of uranium in basement metamorphic rocks of Xiangshan volcanic collapse basin. Uranium Geology 14 (1), 1–6 (in Chinese with English Abstract).
Hu, G.R., Zhang, B.T., 1999. Preliminary study on the Nd-isotopic model ages and the formation age of the metamorphic basement in Central Jiangxi. Uranium Geology. 15 (3), 137–141 (in Chinese with English Abstract).
Hu, R.Z., Bi, X.W., Zhou, M.F., Peng, J.T., Su, W.C., Liu, S., Qi, H.W., 2008. Uranium Met allogenesis in South China and its Relationship to Crustal Extension during the cretaceous to Tertiary. Econ. Geol. 103 (3), 583–598.
Hu, R.-Z., Chen, W.T., Xu, D.-R., Zhou, M.-F., 2017. Reviews and new met allogenic models of mineral deposits in South China: an introduction. J. Asian Earth Sci. 137, 1–8.
Huang, H.Q., Li, X.H., Li, Z.X., Li, W.X., 2015. Formation of the Jurassic South China large Granitic Province: Insights from the genesis of the Jiufeng pluton. Chem. Geol. 401 (0), 43–58.
JGS, 1984. Regional Geology of Jiangxi Province Geological Memoirs. Geological Publishing House. Beijing (921 pp.).
Jiang, Y.-H., Zhu, S.-Q., 2017. Petrogenesis of the late Jurassic peraluminous biotite granites and muscovite-bearing granites in SEChina: geochronological, elemental and Sr–Nd–O–Hf isotopic constraints. Contrib. Mineral. Petrol. 172 (11), 101.
Jiang, X.-Y., Li, X.-H., Collins, W.J., Huang, H.-Q., 2015. U-Pb age and Hf-O isotopes of detrital zircons from Hainan Island: Implications for Mesozoic subduction models. Lithos 239, 60–70.
Jung, S., Pfander, J.A., 2007. Source composition and melting temperatures of orogenic granitoids:constraints from CaO/Na2O, Al2O3/TiO2 and accessory mineral saturation thermometry. Eur. J. Mineral. 19 (6), 859–870.
Kinny, P.D., Maas, R., 2003. Lu-Hf and Sm-Nd isotope systems in zircon. Rev. Mineral. Geochem. 53, 327–341.
Klötzli, U., Klötzli, E., Günes, Z., Kosler, J., 2009. Accuracy of Laser Ablation U-Pb Zircon Dating: results from a Test using five Different Reference Zircons. Geostand. Geoanal. Res. 33 (1), 5–15.
Li, Z.X., 1998. Tectonic History of the Major East Asian Lithospheric Blocks Since the Mid-Proterozoic—A Synthesis. 27. American Geophysical Union, pp. 221–243.

Li, Z.X., Li, X.H., 2007. Formation of the 1300-km-wide intracontinental orogen and postorogenic magmatic province in Mesozoic South China: a flat-slab subduction model. Geology 35 (2), 179–182.
Li, X.H., Li, Z.X., Wingate, M.T.D., Chung, S.L., Liu, Y., Lin, G.C., Li, W.X., 2006. Geochemistry of the 755Ma Mundine well dyke swarm, northwestern Australia: part of a Neoproterozoic mantle superplume beneath Rodinia? Precambrian Res. 146 (1–2), 1–15.
Li, X.H., Li, Z.X., Li, W.X., Liu, Y., Yuan, C., Wei, G.J., Qi, C.S., 2007a. U-Pb zircon, geochemical and Sr-Nd-Hf isotopic constraints on age and origin of Jurassic I- and A-type granites from Central Guangdong, SEChina: a major igneous event in response to foundering of a subducted flat-slab? Lithos 96 (1–2), 186–204.
Li, X.H., Li, W.X., Li, Z.X., 2007b. On the genetic classification and tectonic implications of the early Yanshanian granitoids in the Nanling Range, South China. Chin. Sci. Bull. 52 (14), 1873–1885.
Li, X.H., Li, W.X., Li, Z.X., Liu, Y., 2008. 850-790 Ma bimodal volcanic and intrusive rocks in northern Zhejiang, South China: a major episode of continental rift magmatism during the breakup of Rodinia. Lithos 102 (1–2), 341–357.
Li, X.H., Li, W.X., Li, Z.X., Lo, C.H., Wang, J., Ye, M.F., Yang, Y.H., 2009. Amalgamation between the Yangtze and Cathaysia Blocks in South China: Constraints from SHRIMPU-Pb zircon ages, geochemistry and Nd-Hf isotopes of the Shuangxiwu volcanic rocks. Precambrian Res. 174 (1–2), 117–128.
Li, X.H., Li, Z.X., He, B., Li, W.X., Li, Q.L., Gao, Y.Y., Wang, X.C., 2012. The early Permian active continental margin and crustal growth of the Cathaysia Block: in situ U–Pb, Lu–Hf and O isotope analyses of detrital zircons. Chem. Geol. 328 (0), 195–207.
Li, X.H., Liu, X., Liu, Y., Su, L., Sun, W., Huang, H., Yi, K., 2015. Accuracy of LA-ICPMS zircon U-Pb age determination: an inter-laboratory comparison. SCIENCE CHINA Earth Sciences. 58 (10), 1722–1730.
Liang, X.R., Wei, G.J., Li, X.H., Liu, Y., 2003. Precise measurement of $^{143}Nd/^{144}Nd$ and Sm/Nd ratios using multiple-collectors inductively couple plasma-mass spectrometer (MC-ICP-MS). Geochimica 32, 91–96 (in Chinese with English abstract).
Lin, W.W., Peng, L.J., 1994. The estimation of Fe^{3+} and Fe^{2+} contents in amphibole and biotite from EMPA data. Journal of Changchun University of Earth Science. 24 (2), 155–162 (in Chinese with English abstract).
Liu, Y., Hu, Z., Gao, S., Günther, D., Xu, J., Gao, C., Chen, H., 2008. In situ analysis of major and trace elements of anhydrous minerals by LA-ICP-MS without applying an internal standard. Chem. Geol. 257 (1), 34–43.
Ludwig, K.R., 2003. Isoplot: a geochronological toolkit for Microsoft Excel. Berkeley Geochronology Center Special Publication 4, 1–67.
Luo, Z.G., Wang, Y.J., Zhang, F.F., Zhang, A.M., Zhang, Y.Z., 2010. LA-ICPMS zircon U-Pb dating for Baimashan and Jintan Indosinian graniticp plutons and its petrogeneitc implications. Geotectonica et Met alleognia. 34 (2), 282–290 (in Chinese with English abstract).
Maniar, P.D., Piccoli, P.M., 1989. Tectonic discrimination of granitoids. Geol. Soc. Am. Bull. 101 (5), 635–643.
McArthur, J.M., 1994. Recent trends in strontium isotope stratigraphy. Terra Nova 6 (4), 331–358.
Middlemost, E.A.K., 1994. Naming materials in the magma/igneous rock system. Earth Sci. Rev. 37 (3–4), 215–224.
Miller, C.F., 1981. Stoddard.E. F, Bradfish.L. J,Dollase. W. A. Composition of plutonic muscovite 19, 25–34.
Miller, C.F., McDowell, S.M., Mapes, R.W., 2003. Hot and cold granites? Implications of zircon saturation temperatures and preservation of inheritance. Geology 31 (6), 529–532.
Pearce, N.J.G., Perkins, W.T., Westgate, J.A., Grrton, M.P., Jackson, S.E., Neal, C.R., Chenery, S. P., 1997. A compilation of new and published major and trace element data for NIST SRM 610 and NIST SRM 612 glass reference materials. Geostand. Newslett. 21, 115–144.
Profeta, L., Ducea, M.N., Chapman, J.B., Paterson, S.R., Gonzales, S.M.H., Kirsch, M., Petrescu, L., Decelles, P.G., 2015. Quantifying crustal thickness over time in magmatic arcs. Sci. Rep. 5, 17786.
Qi, C.S., Deng, X.G., Li, W.X., Li, X.H., Yang, Y.H., Xie, L.W., 2007. Origin of the DarongshanShiwandashan S-type granitoid belt from southeastern Guangxi: geochemical and SrNd-Hf isotopic constraints. Acta Petrol. Sin. 23, 403–412 (in Chinese with English abstract).
Scherer, E., Münker, C., Mezger, K., 2001. Calibration of the Lutetium-Hafnium Clock. Science 293 (5530), 683–687.
Shen, W.Z., Zhu, J.C., Liu, C.S., Xu, S.j., Ling, H.F., 1993. Sm-Nd isotopic study of basement metamorphic rocks in South China and its constraint on material sources of granitoids. Acta Petrol. Sin. 9 (2), 115–124 (in Chinese with English abstract).
Shen, W., Yu, J., Zhao, L., Chen, Z., Lin, H., 2003. Nd isotopic characteristics of post-Archean sediments from the Eastern Nanling Range: evidence for crustal evolution. Chin. Sci. Bull. 48 (16), 1679–1685.
Speer, J.A., 1984. Micas in Igneous Rocks. Rev. Mineral. 13, 299–356.
Sun, S.-s, McDonough, W.F., 1989. Chemical and isotopic systematics of oceanic basalts: implications for mantle composition and processes. Geol. Soc. Lond., Spec. Publ. 42 (1), 313–345.
Sylvester, P.J., 1998. Post-collisional strongly peraluminous granites. Lithos 45 (1–4), 29–44.
Tanaka, T., Togashi, S., Kamioka, H., Amakawa, H., Kagami, H., Hamamoto, T., Yuhara, M., Orihashi, Y., Yoneda, S., Shimizu, H., Kunimaru, T., Takahashi, K., Yanagi, T., Nakano, T., Fujimaki, H., Shinjo, R., Asahara, Y., Tanimizu, M., Dragusanu, C., 2000. JNdi-1: a neodymium isotopic reference in consistency with LaJolla neodymium. Chem. Geol. 168 (3), 279–281.
Tang, G.-J., Wang, Q., Zhang, C., Wyman, D.A., Dan, W., Xia, X.-P., Chen, H.-Y., Zhao, Z.-H., 2017. Sr-Nd-Hf-O isotope geochemistry of the Ertaibei pluton, East Junggar, NWChina: Implications for development of a crustal-scale granitoid pluton and crustal growth. Geochem. Geophys. Geosyst. 18 (9), 3340–3358.
Tu, X.L., Zhang, H., Deng, W.F., Ling, M.X., Liang, H.Y., Liu, Y., Sun, W.D., 2011. Application of RESOlution in-situ laser ablation ICP-MS in trace element analyses. Geochemica 40 (1), 83–98 (in Chinese with English abstract).
Wang, Y.J., Fan, W.M., Zhang, G.W., Zhang, Y.H., 2013. Phanerozoic tectonics of the South China Block: Key observations and controversies. Gondwana Res. 23 (4), 1273–1305.
Wei, G.J., Liang, X.R., Li, X.H., Liu, Y., 2002. Precise measurement of Sr isotopic compositions of liquid and solid base using (LA) MC-ICP-MS. Geochimica 31, 295–305 (in Chinese with English abstract).
Whalen, J.B., 1985. Geochemistry of an Island-Arc Plutonic Suite: the Uasilau-Yau Yau Intrusive complex, New Britain, P.N.G. J. Petrol. 26 (3), 603–632.
Wones, D.R., Eugster, H.P., 1965. Stability of Biotite:Experiment Theory and Application. Am. Mineral. 50 (9), 1228–1271.
Woodhead, J., Hergt, J., Shelley, M., Eggins, S., Kemp, R., 2004. Zircon Hf-isotope analysis with an excimer laser, depth profiling, ablation of complex geometries, and concomitant age estimation. Chem. Geol. 209 (1), 121–135.
Wu, F.Y., Yang, Y.H., Xie, L.W., Yang, J.H., Xu, P., 2006. Hf isotopic compositions of the standard zircons and baddeleyites used in U-Pb geochronology. Chem. Geol. 234, 105–126.
Wu, F.Y., Li, X.H., Yang, J.H., Zheng, Y.F., 2007. Discussions on the petrogenesis of granites. Acta Petrol. Sin. 23 (6), 1217–1238 (in Chinese with English abstract).
Zhang, Z.H., Zhang, B.T., 1991. On the Uranium-Bearing Granites and their Related Uranium Deposits in South China. Vol. 258. Atomic Energy Press, Beijing (in Chinese with English abstract).
Zhang, L., Ren, Z.Y., Nichols, A.R.L., et al., 2014. Lead isotope analysis of melt inclusions by LA-MC-ICP-MS. J. Anal. At. Spectrom. 29 (8), 1393–1405.
Zhang, L., Chen, Z., Li, S., Santosh, M., Huang, G., Tian, Z., 2017. Isotope geochronology, geochemistry, and mineral chemistry of the U-bearing and barren granites from the Zhuguangshan complex, South China: Implications for petrogenesis and uranium mineralization. Ore Geol. Rev. 91, 1040–1065.
Zhao, K.D., Jiang, S.Y., Dong, C.Y., Chen, W.F., Chen, P.R., Ling, H.F., Zhang, J., Wang, K.X., 2011. Uranium-bearing and barren granites from the Taoshan complex, Jiangxi Province, South China: Geochemical and petrogenetic discrimination and exploration significance. J. Geochem. Explor. 110 (2), 126–135.
Zhao, K.D., Jiang, S.Y., Chen, W.F., Chen, P.R., Ling, H.F., 2013a. Zircon U–Pb chronology and elemental and Sr–Nd–Hf isotope geochemistry of two Triassic A-type granites in South China: Implication for petrogenesis and Indosinian transtensional tectonism. Lithos 160–161 (0), 292–306.
Zhao, K.D., Li, J.R., Ling, H.F., Chen, P.R., Chen, W.F., Sun, T., 2013b. Geochronology, geochemistry and petrogenesis of two-stage Indosinian granites from the Xiajiang uranium ore deposit, Jiangxi Province: Implication for Indosinian tectonics and genesis of uranium-bearing granites in South China. Acta Petrol. Sin. 29 (12), 4349–4361 (in Chinese with English abstract).
Zhao, Z.-F., Gao, P., Zheng, Y.-F., 2015. The source of Mesozoic granitoids in South China: Integrated geochemical constraints from the Taoshan batholith in the Nanling Range. Chem. Geol. 395 (0), 11–26.
Zhao, K.-D., Jiang, S.-Y., Ling, H.-F., Sun, T., Chen, W.-F., Chen, P.-R., Pu, W., 2016. Late Triassic U-bearing and barren granites in the Miao'ershan batholith, South China: Petrogenetic discrimination and exploration significance. Ore Geol. Rev. 77, 260–278.
Zhao, Z., Miao, B., Xu, Z., Lu, J., Liu, L., Zuo, C., Lu, R., Wang, H., 2017. Petrogenesis of two types of late Triassic granite from the Guandimiao complex, southern Hunan Province, China. Lithos 282–283, 403–419.
Zhou, X.M., Sun, T., Shen, W.Z., Shu, L.S., Niu, Y.L., 2006. Petrogenesis of Mesozoic granitoids and volcanic rocks in South China: a response to tectonic evolution. Episodes 29 (1), 26–33.